**For the Supporting Information**

Cyclic Polylactide initiated by a Lithium Anthraquinoid: Understanding the selectivity through DFT and Diffusion NMR

*Cristina Ruiz Martínez,*[a,†] *Juana M. Pérez,*[a,†] *Francisco M. Arrabal-Campos,*[a] *María Batuecas,*[a] *Manuel A. Ortuño,*[b,c] *and Ignacio Fernández*[*,a]

[a] Department of Chemistry and Physics, Research Centre CIAIMBITAL, University of Almería, Ctra. Sacramento, s/n, 04120, Almería, Spain. E-mail: ifernan@ual.es

[b] Institute of Chemical Research of Catalonia (ICIQ), The Barcelona Institute of Science and Technology (BIST), Av. Països Catalans 16, 43007 Tarragona, Spain.

[c] Centro Singular de Investigación en Química Biolóxica e Materiais Moleculares (CIQUS), Universidad de Santiago de Compostela, 15782 Santiago de Compostela, Spain.

**Index**


**Figure S1**. Kinetic profiles S3

**Figure S2**. $^{1}$H NMR and homonuclear decoupled spectra S4

**Figure S3**. MALDI-TOF spectra of cyclic L-PLA S5

**Figure S4**. MALDI-TOF spectra of cyclic *rac*-PLA S6

**Figure S5**. MALDI-TOF spectra of linear + cyclic L-PLA S7

**Figure S6**. DRIFT spectra of commercial linear PLA and cPLA S8-9

**Figure S7-S8**. Diffusion NMR Stejskal-Tanner plots S10-S11

**Figure S9**. $^{1}$H NMR spectrum of L-cPLA S12

**Figure S10**. Inverse-gated $^{13}$C{$^{1}$H} spectrum of L-cPLA S12

**Figure S11**. $^{1}$H NMR spectrum of cyclic *rac*-PLA S13

**Figure S12**. $^{1}$H Homodecoupled NMR spectrum of *rac*-cPLA S13

**Figure S13**. Inverse-gated $^{13}$C NMR spectra of *rac*-cPLA S14

**Figure S14**. $^{1}$H NMR spectrum of cyclic *rac*-PLA obtained in DCM S14

**Figure S15**. $^{1}$H Homodecoupled NMR spectrum of *rac*-cPLA obtained in DCM S15

**Figure S16**. Inverse-gated $^{13}$C NMR spectra of *rac*-cPLA obtained in DCM S15

**Table S1.** $^{1}$H and $^{13}$C NMR intensities (%) of tetrad fractions S16

**Table S2**. Theoretical and experimental MW values for cPLAs S17

**Table S3.** Diffusion coefficients and weight-average molecular weights S18

**Figure S17**. PMMA chromatograms S19

**Figure S18**. SEC Calibration curve based on six PMMA standards S20

**Figure S19**. SEC mass distribution curves for entries 1-4, Table 3 S21

**Figure S20**. SEC mass distribution curves for entries 5-7, Table 3 S22

**Figure S21**. Comparison between Mw retrieved from NMR and SEC S23

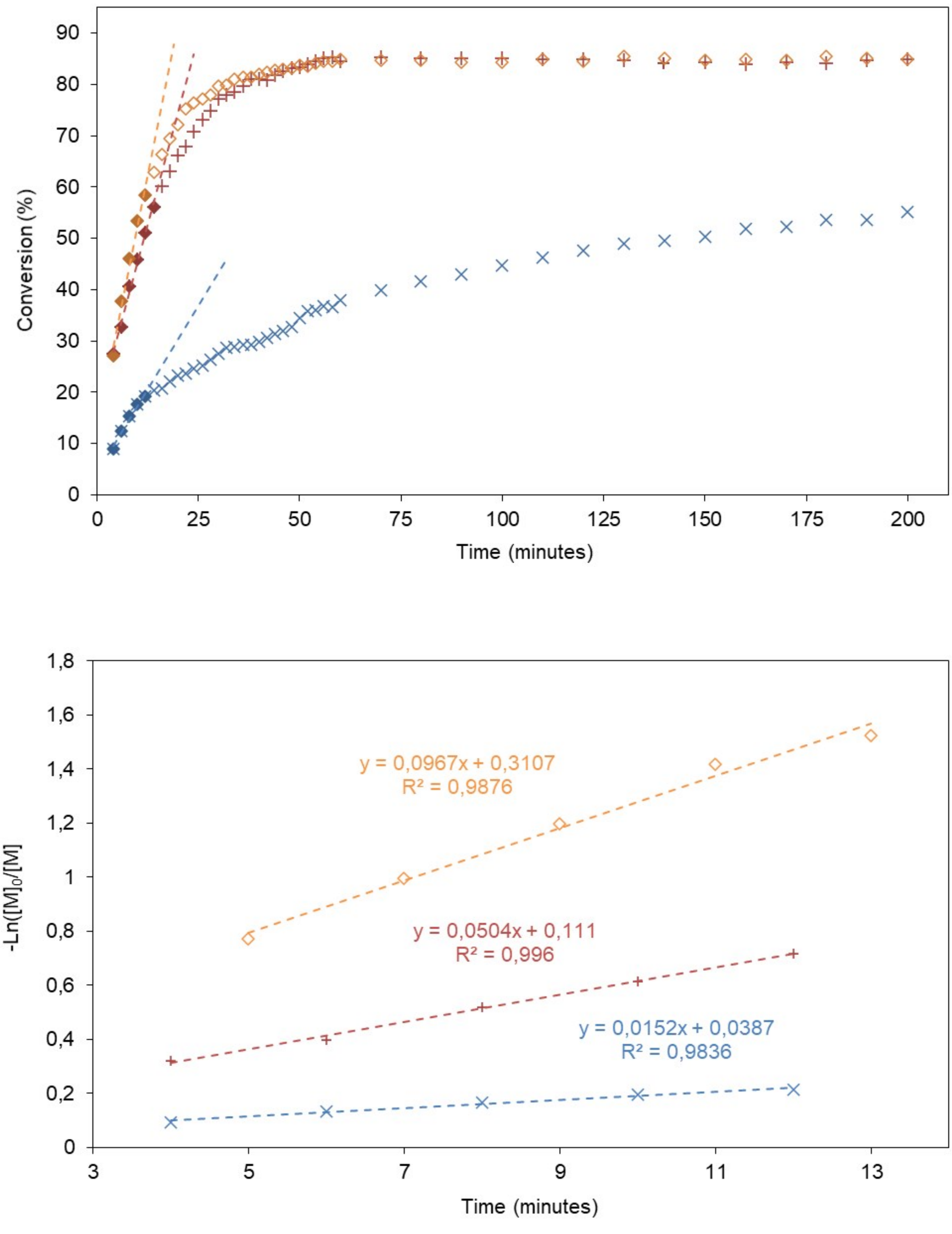


**Figure S1**. Kinetic profiles (top) and -Ln(M/M$_0$) dependence (bottom) for the catalytic ROP of L-lactide with LiHMDS (x), one-pot (+) and complex **6** (◊) at 25 ºC in THF.

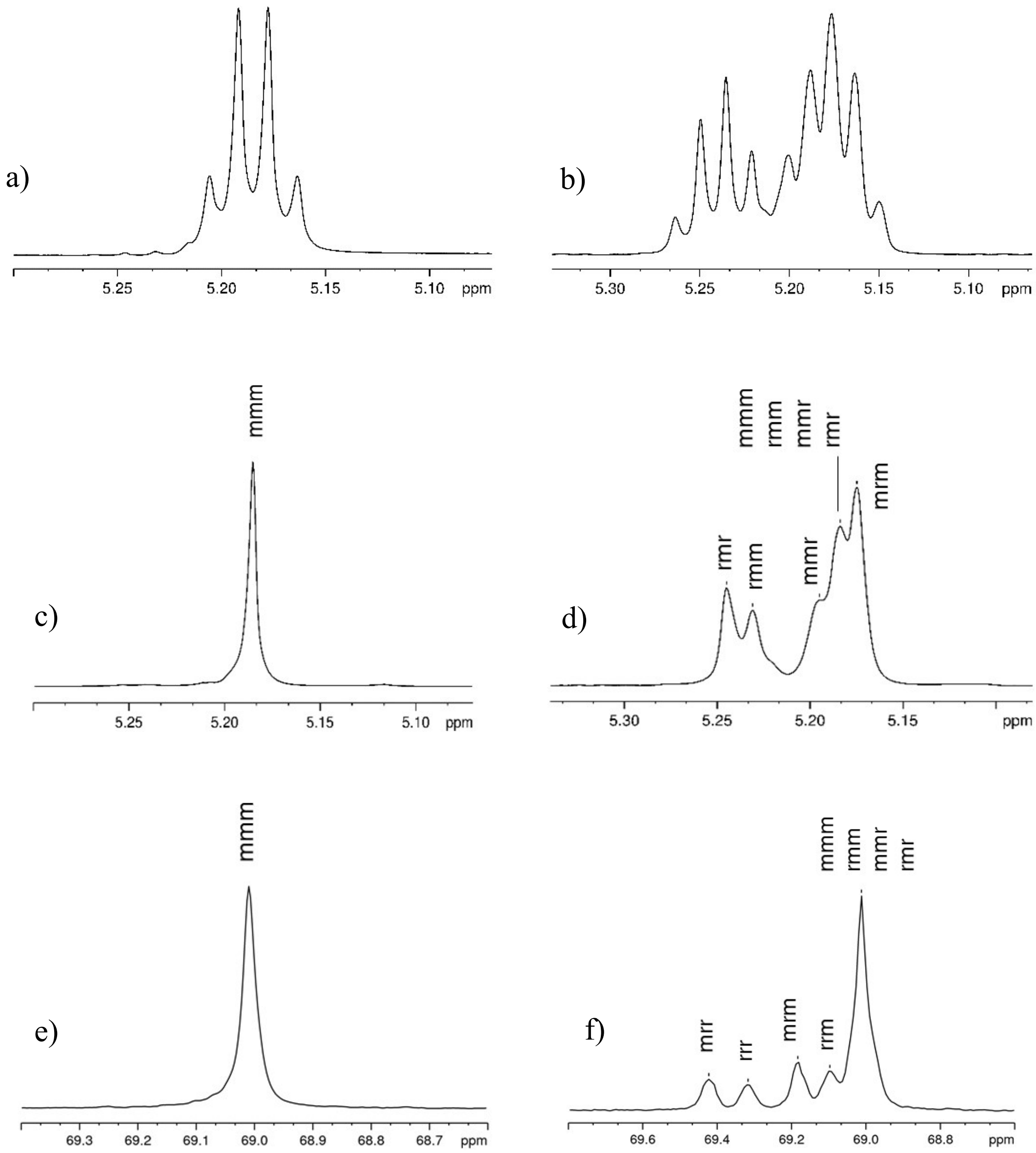


**Figure S2**. a) $^{1}H$ NMR spectrum of L-cPLA; b) $^{1}H$ NMR spectrum *rac*-cPLA; c) Homodecoupled $^{1}H$ NMR spectrum of L-cPLA; d) Homodecoupled $^{1}H$ NMR spectrum of *rac*-cPLA; e) Inverse-gated $^{13}C\{1H\}$ NMR spectrum of L-cPLA and f) Inverse-gated $^{13}C\{^{1}H\}$ NMR spectrum of *rac*-cPLA. Decoupled peaks are labeled with their corresponding stereosequences.

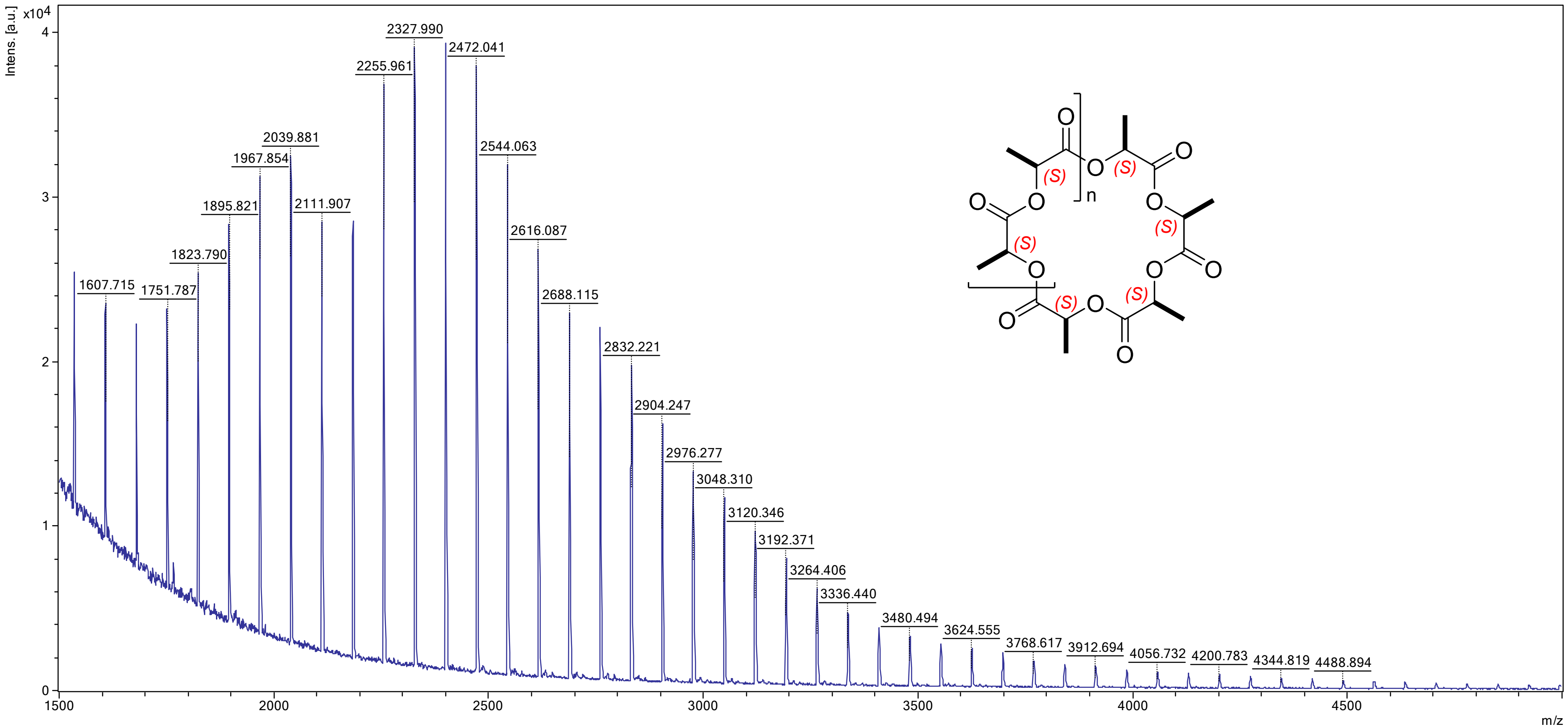


**Figure S3**. MALDI-TOF spectra of cyclic L-PLA obtained using **6** as catalyst in DCM at a 50:1 $[LA]_0/[Cat]$ ratio.

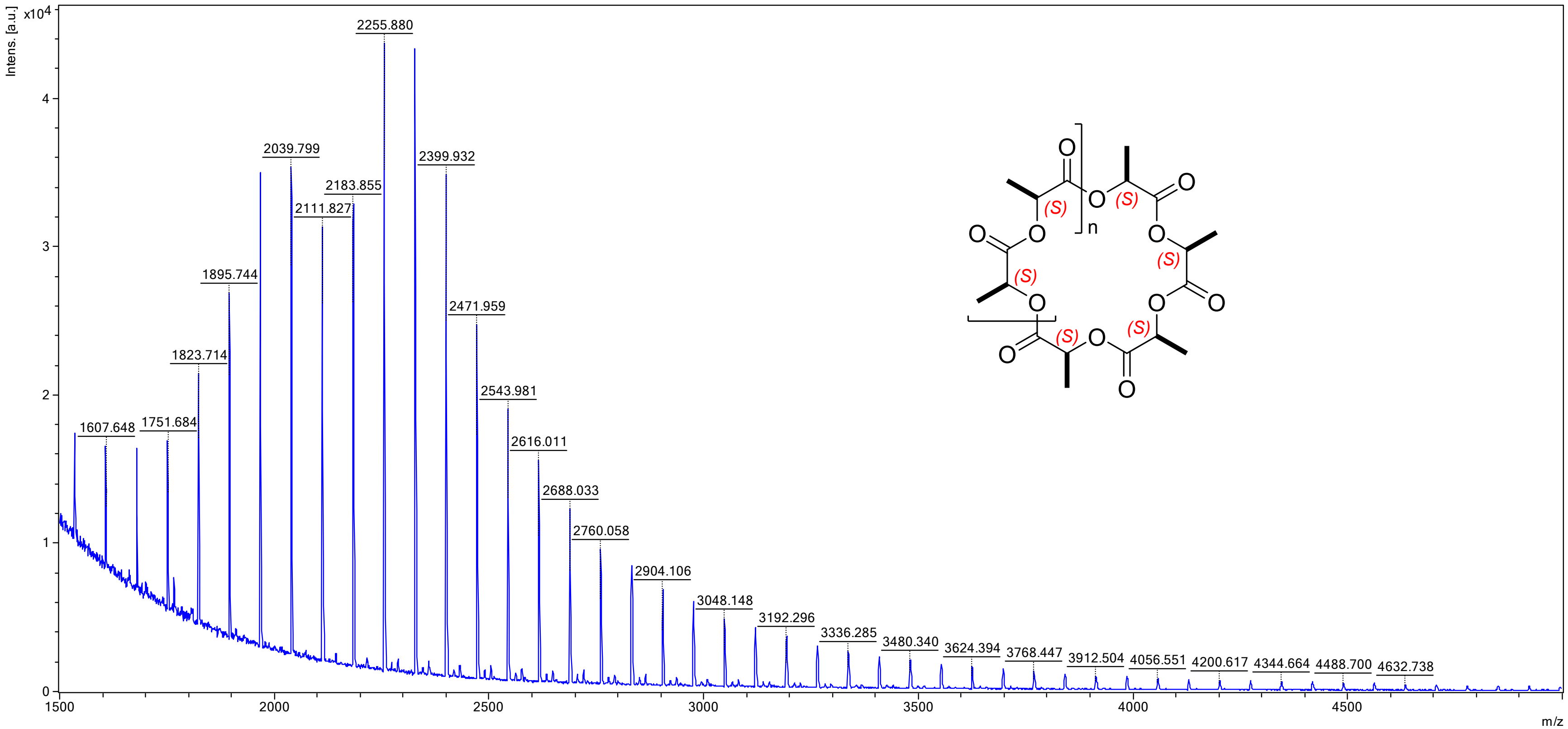


**Figure S4**. MALDI-TOF spectra of cyclic *rac*-PLA obtained using **6** as catalyst in DCM at a 50:1 $[LA]_0/[Cat]$ ratio.

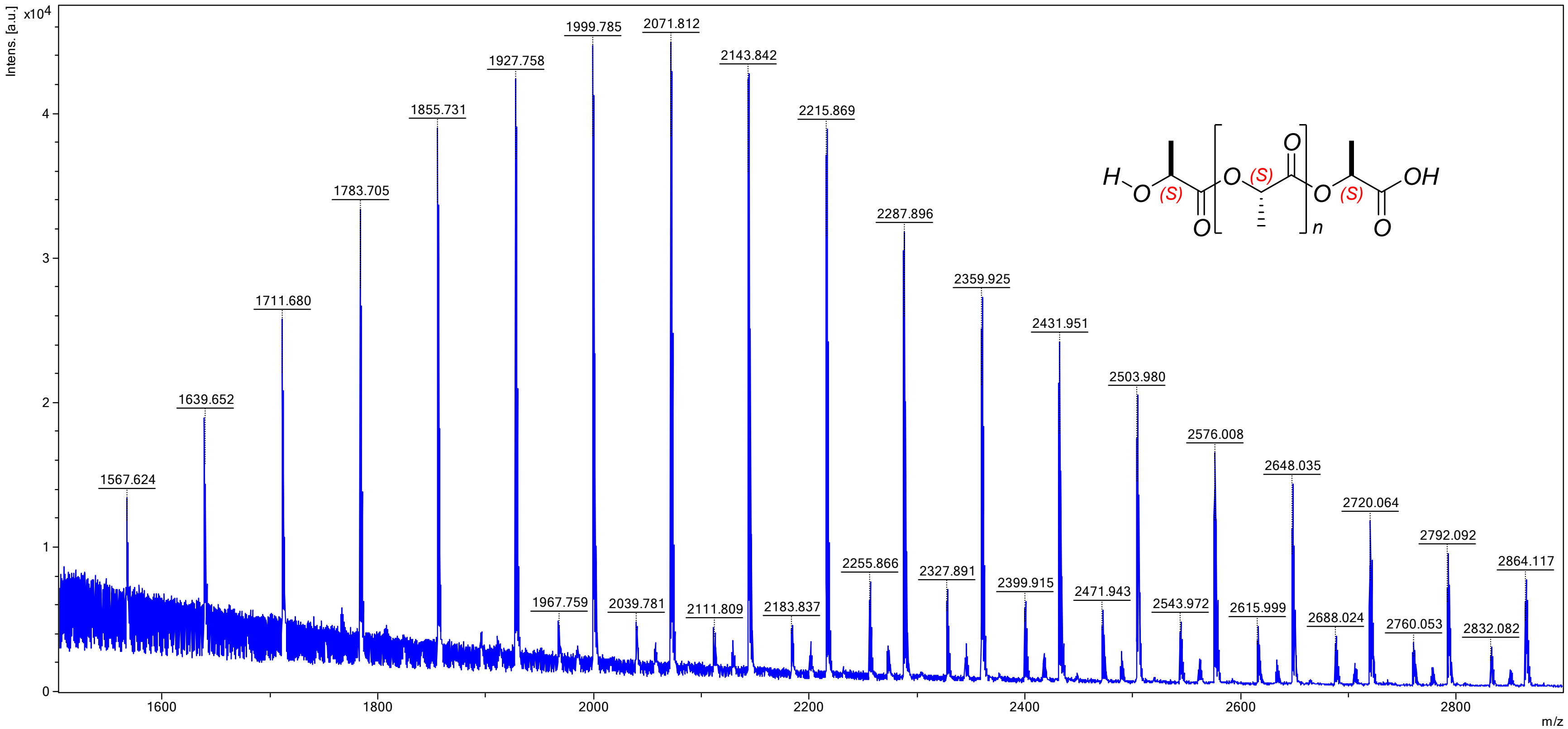


**Figure S5**. MALDI-TOF spectra of L-PLA obtained using LiHMDS as catalyst in DCM at a 50:1 $[LA]_0/[Cat]$ ratio.

## DRIFT SPECTRA

Spectra were always obtained at room temperature and after placing the samples at least 8 h under vacuum. The DRIFT spectra of PLA revealed characteristic absorption peaks of ester (1758 and 1196 $cm^{-1}$ for –COO-and –CO-, respectively) and $–CH_3$ (stretching) group (2999 and 2949 $cm^{-1}$) that are slightly shifted to lower wavenumbers compared to free LA (Figure S6). As expected, within the intense and sharp absorption peak ascribed to the C=O stretching is observed its overtone at 3508 $cm^{-1}$ together with two OH bands located at 3649 and 3559 $cm^{-1}$ associated to reticular or coordinated water within the polymer chains. Interestingly, these three bands are absent in the attenuated total reflectance (ATR) spectra for both linear and cyclic polymers. The linear polymer affords in the DRIFT measurement a large broad signal in the region above 3200 $cm^{-1}$ probably associated to terminal hydroxylic ends, together with an extra signal at 1563 $cm^{-1}$ exclusively observed in the linear polymer.

The presence of residual monomer in the final product can cause problems such as lowering mechanical strength and thermal stability. From an examination of the fingerprint region of spectra obtained from our catalysis, the lack of LA could be ascertained in the mid-IR region by the absence of an isolated peak at a wavenumber of 935 $cm^{-1}$ attributed to the COO ring breathing mode of the LA. These observations verify our NMR findings of pure cPLA.

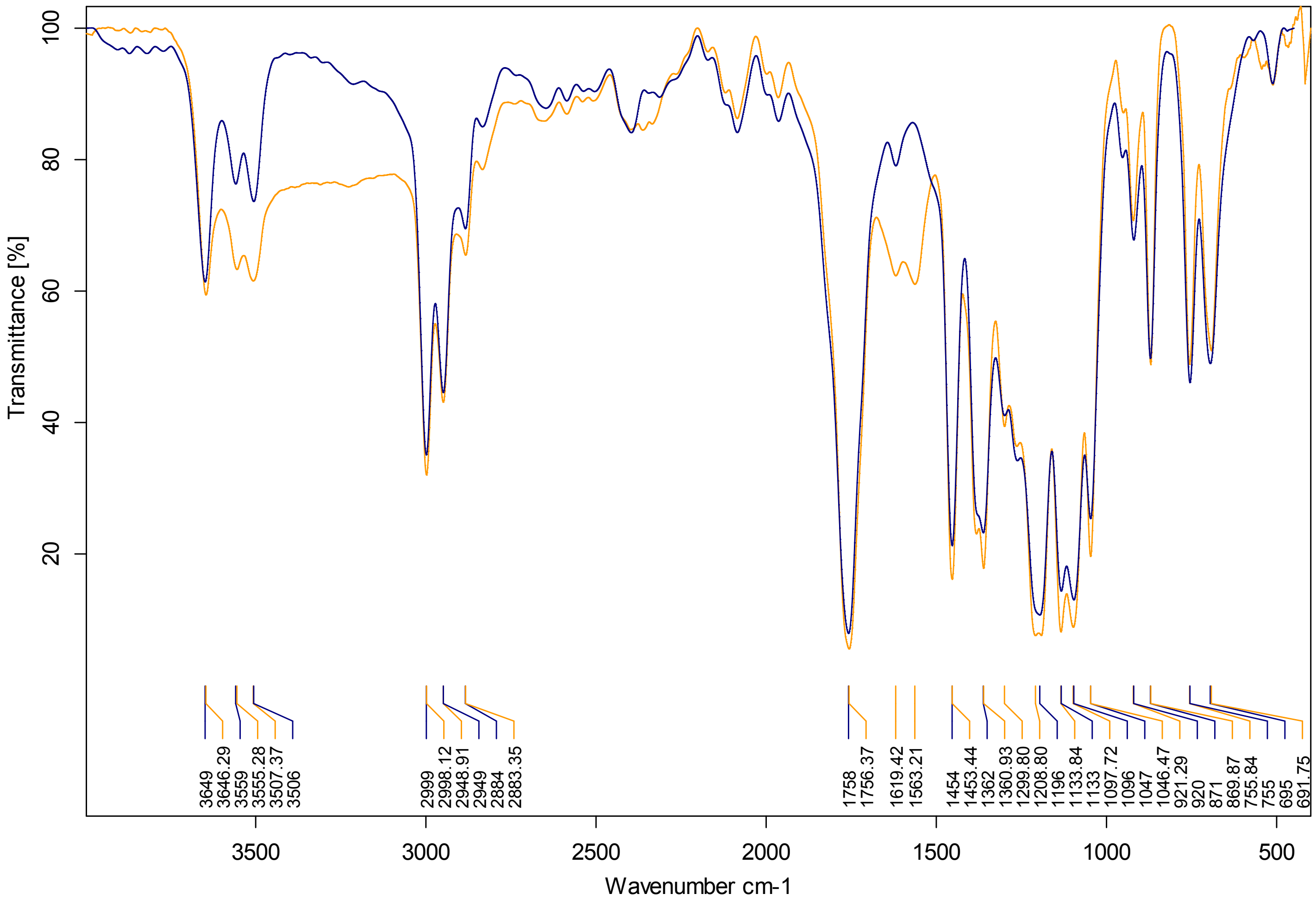


**Figure S6**. DRIFT spectra of commercial linear PLA (**orange**) and cPLA (**blue**) obtained in the presence of complex **6**, in THF at 298 K and 50:1 $[LA]_0/[Cat]$ ratio.

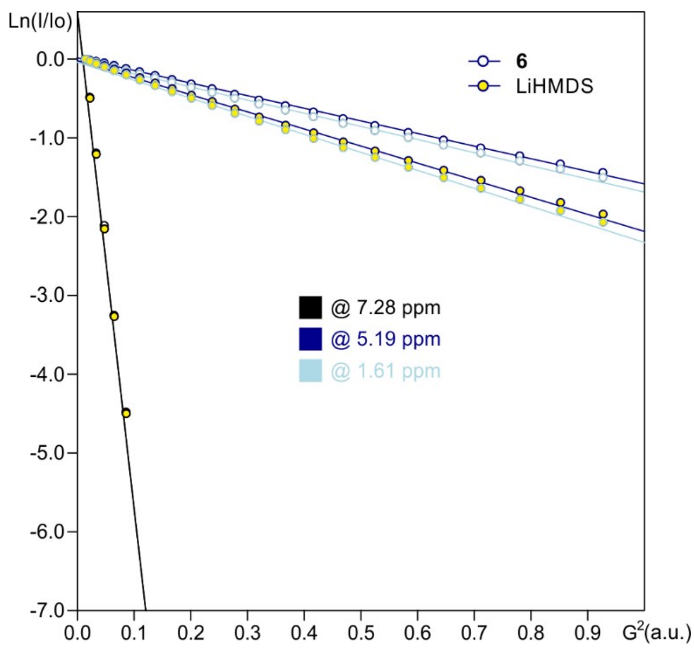


**Figure S7**. Stejskal-Tanner plots from $^{1}$H PGSE NMR diffusion experiments in $CDCl_3$at 297 K using the stimulated echo with bipolar pair pulses (stebpgp1s1d) sequence for cyclic L-PLA (1.5 mg in 0.5 mL) obtained with LiHMDS or complex **6** as catalyst both at 50:1[LA]$_0$/[Cat] ratio. The solid lines represent linear least-squares fits to the experimental data.

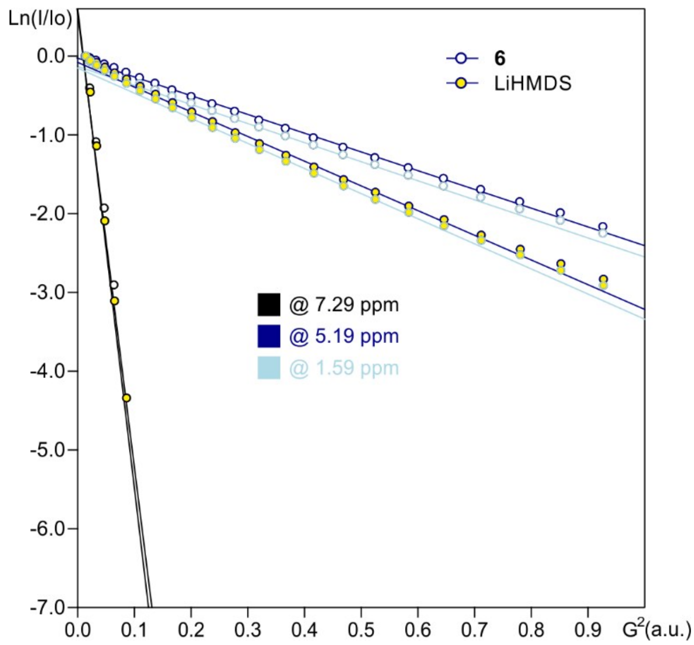


**Figure S8**. Stejskal-Tanner plots from [1]H PGSE NMR diffusion experiments in $CDCl_3$at 297 K using the stimulated echo with bipolar pair pulses (stebpgp1s1d) sequence for cyclic *rac*-PLA (1.5 mg in 0.5 mL) obtained with LiHMDS or complex **6** as catalyst both at 50:1 $[LA]_0/[Cat]$ ratio. The solid lines represent linear least-squares fits to the experimental data.

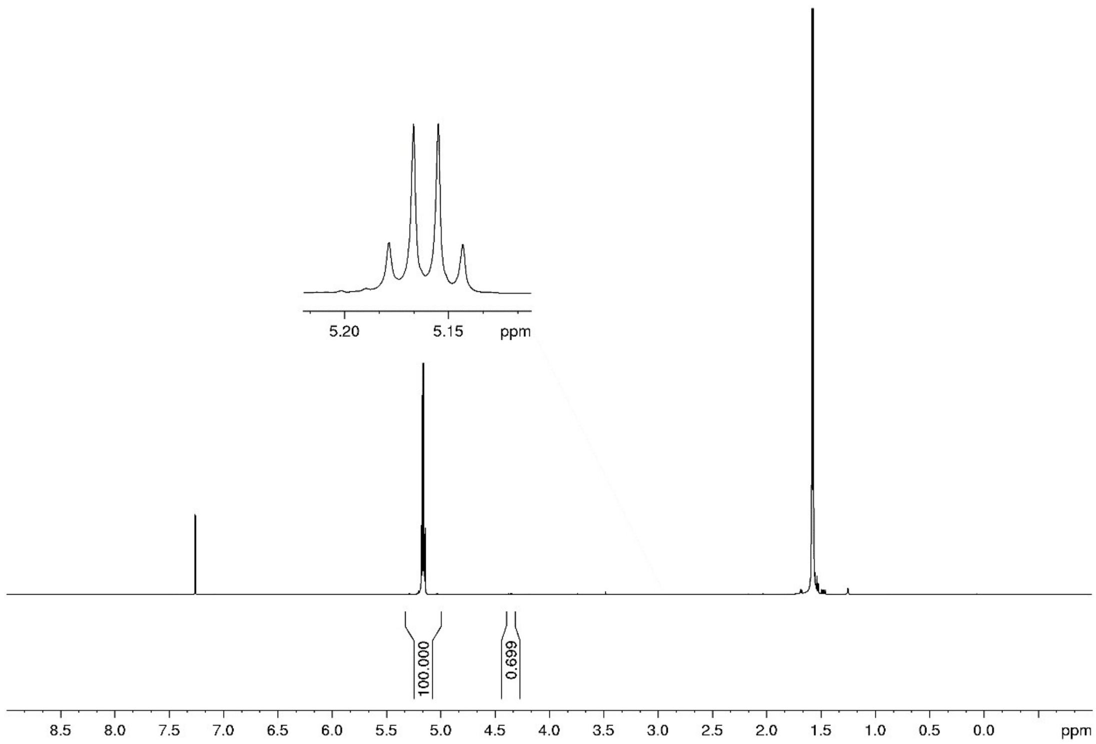


**Figure S9**. $^{1}H$ NMR spectrum (500.13 MHz, $CDCl_3$) of cyclic L-PLA obtained with **6** at 50:1 $[LA]_0$/[Cat] ratio in THF at room temperature.

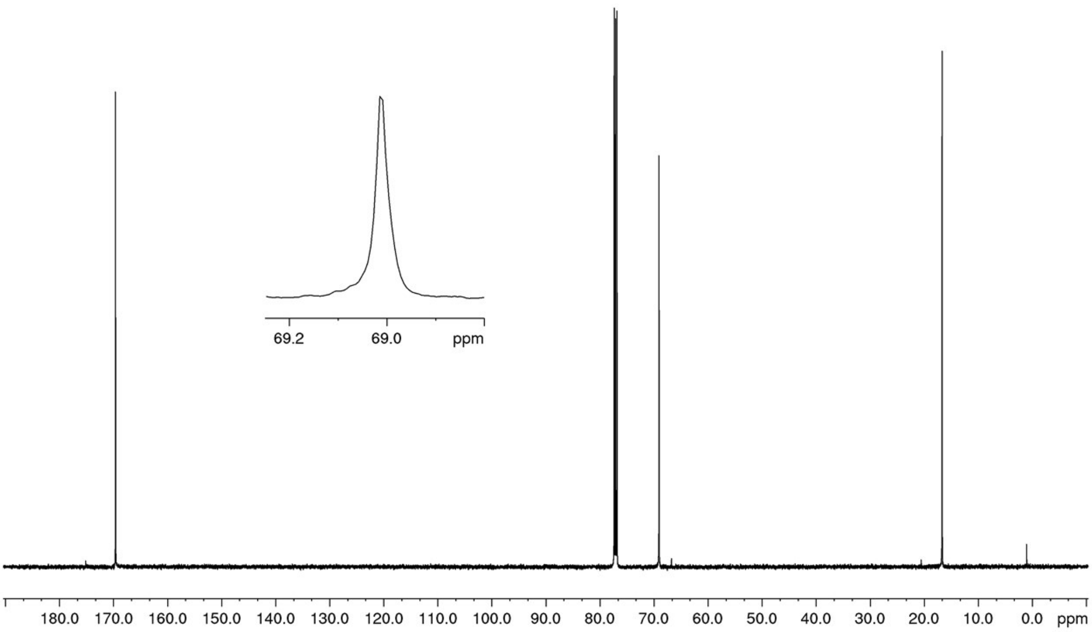


**Figure S10**. Inverse-gated $^{13}C\{^{1}H\}$ spectrum (125.76 MHz, $CDCl_3$) of cyclic L-PLA obtained with **6** at 50:1 $[LA]_0$/[Cat] ratio in THF at room temperature.

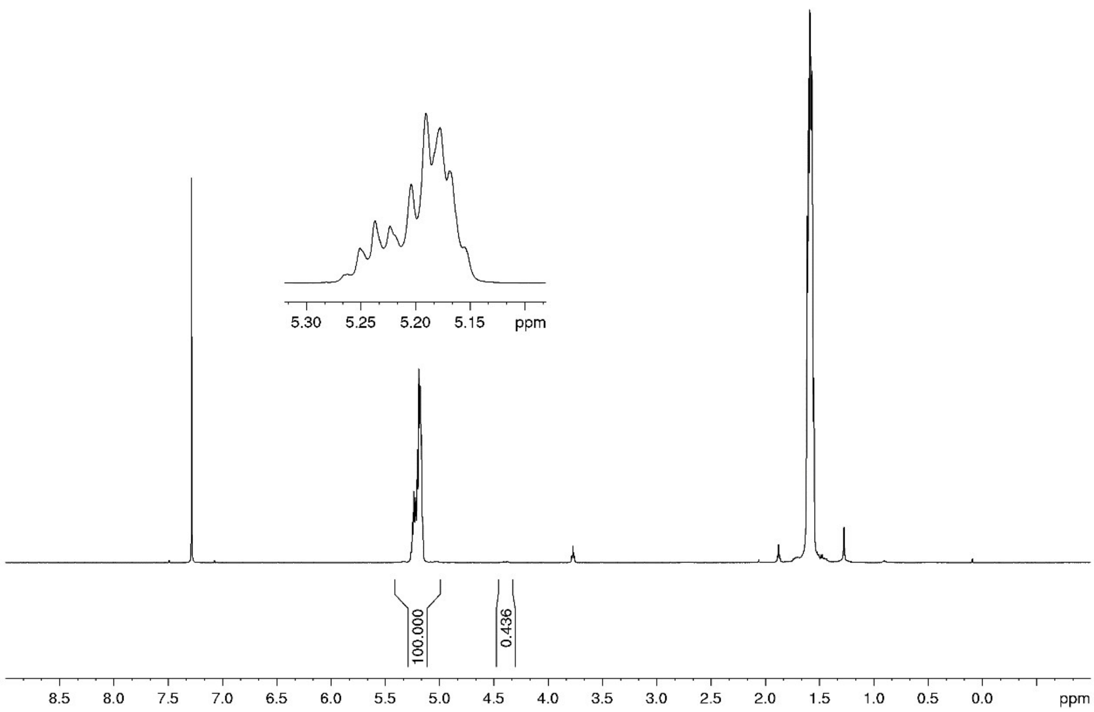


**Figure S11**. $^{1}$H NMR spectrum (500.13 MHz, $CDCl_3$) of cyclic *rac*-PLA obtained with **6** at 50:1 $[LA]_0$/[Cat] ratio in THF at room temperature.

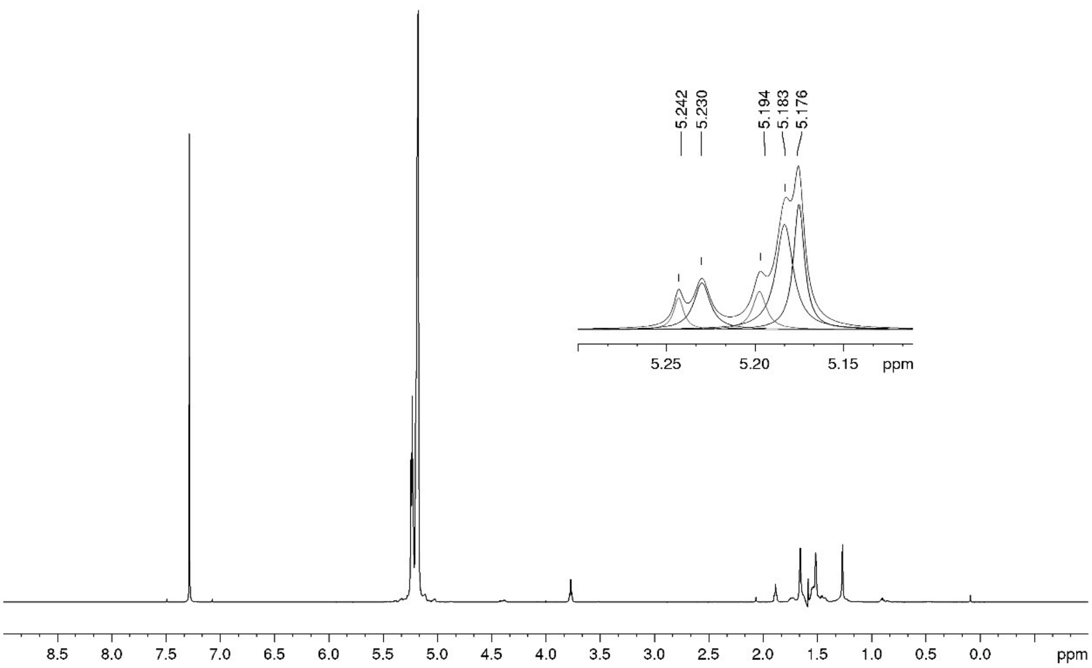


**Figure S12**. Homodecoupled $^{1}$H NMR spectrum (500.13 MHz, $CDCl_3$) of cyclic *rac*-PLA obtained with **6** at 50:1 $[LA]_0$/[Cat] ratio in THF at room temperature.

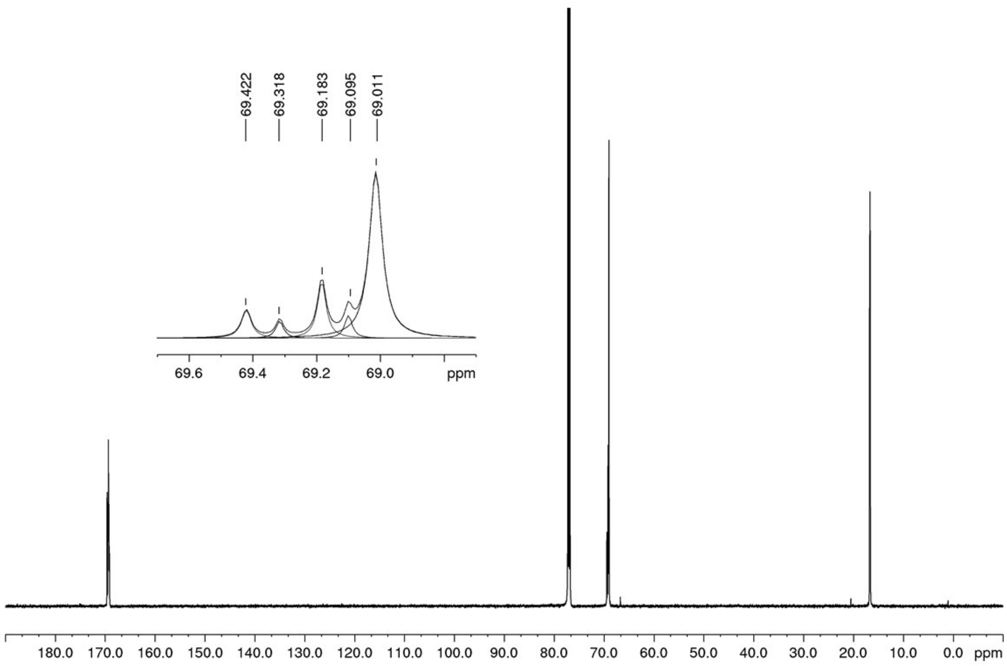


**Figure S13**. Inverse-gated $^{13}C\{^1H\}$ spectrum (125.76 MHz, $CDCl_3$) of cyclic *rac*-PLA obtained with **6** at 50:1 $[LA]_0/[Cat]$ ratio in THF at room temperature.

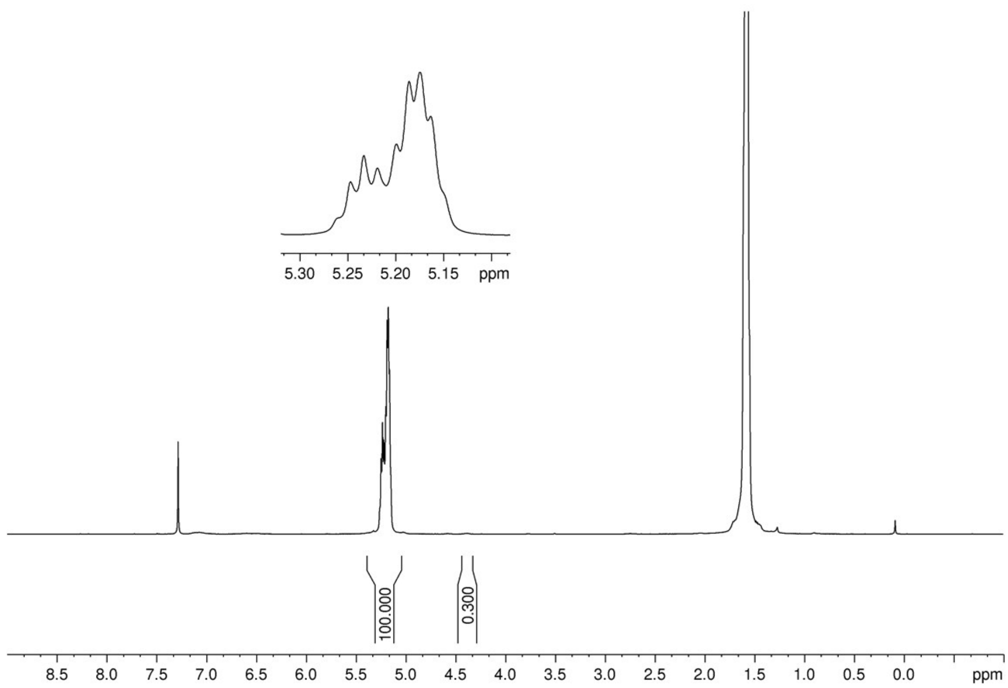


**Figure S14**. $^1H$ NMR spectrum (500.13 MHz, $CDCl_3$) of cyclic *rac*-PLA obtained with **6** at 50:1 $[LA]_0/[Cat]$ ratio in DCM at room temperature.

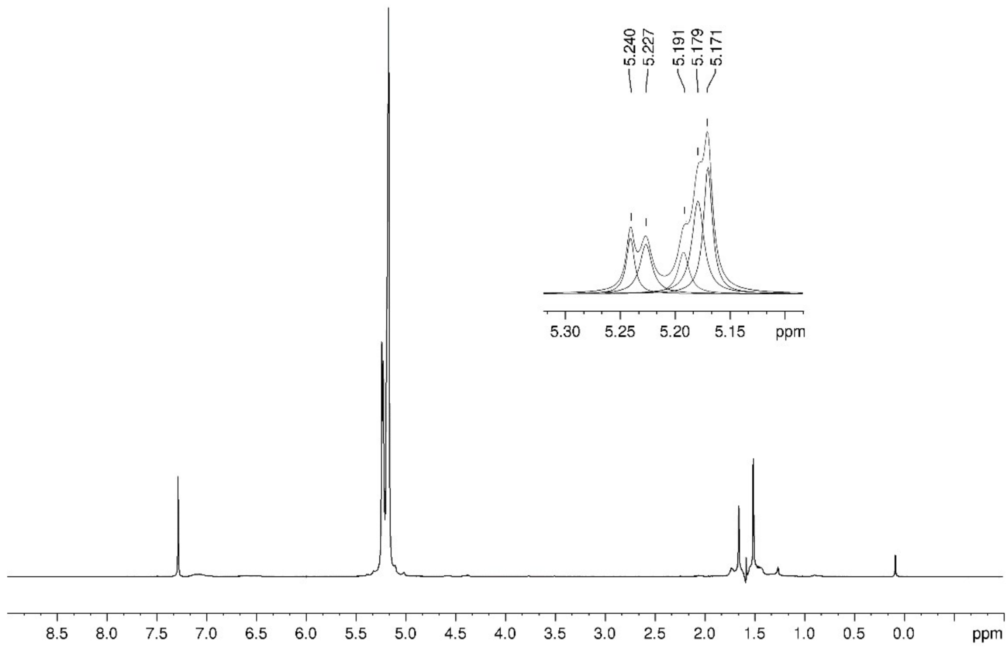


**Figure S15**. Homodecoupled $^{1}H$ NMR spectrum (500.13 MHz, $CDCl_3$) of cyclic *rac*-PLA obtained with **6** at 50:1 $[LA]_0/[Cat]$ ratio in DCM at room temperature.

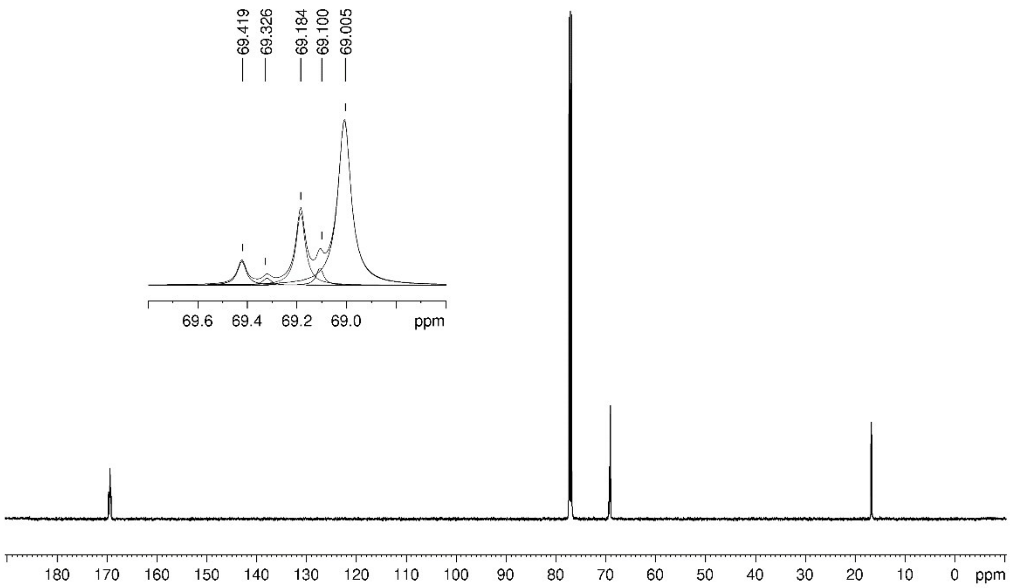


**Figure S16**. Inverse-gated $^{13}C\{^{1}H\}$ spectrum (125.76 MHz, $CDCl_3$) of cyclic *rac*-PLA obtained with **6** at 50:1 $[LA]_0/[Cat]$ ratio in DCM at room temperature.

**Table S1**. $^{1}H$ and $^{13}C$ NMR intensities (%) of tetrad fractions calculated via signal deconvolution of the methine signal.

| | rmr (sis) | rmm (sii) | mmr (iis) | mmm (iii)<br>rrr (sss)<br>rrm (ssi)<br>mrr (iss) | mrm (isi) |
|---|---|---|---|---|---|
| Tacticity[a] | ht | sb it | sb it | it | ht |
| $\delta_H$ (ppm) | 5.23 | 5.22 | 5.18 | 5.17 | 5.16 |
| L-/LiHMDS | - | - | - | 100 | - |
| L-/**6** | - | - | - | 100 | - |
| *rac*-/LiHMDS | 8.9 | 14.6 | 11.8 | 37.8 | 27.0 |
| *rac*-/LiHMDS[b] | 17.0 | 13.1 | 11.8 | 27.3 | 30.8 |
| *rac*-/**6**(50:1) | 6.6 | 16.0 | 10.9 | 37.9 | 28.6 |
| *rac*-/**6**(50:1)[b] | 12.2 | 16.1 | 12.2 | 29.7 | 29.9 |
| *rac*-/**6**(75:1) | 7.0 | 15.6 | 11.0 | 38.2 | 28.2 |
| *rac*-/**6**(100:1) | 7.0 | 15.6 | 10.5 | 38.4 | 28.5 |
| *rac*-/**6**(150:1) | 6.9 | 15.8 | 11.1 | 38.4 | 27.9 |
| | mrr (iss) | rrr (sss) | mrm (isi) | rrm (ssi) | mmm (iii)<br>rmm (sii)<br>mmr (iis)<br>rmr (sis) |
| $\delta_C$ (ppm) | 69.4 | 69.3 | 69.2 | 69.1 | 69.0 |
| L-/LiHMDS | - | - | - | - | 100 |
| L-/**6** | - | - | - | - | 100 |
| *rac*-/LiHMDS | 8.6 | 4.1 | 15.3 | 5.3 | 66.7 |
| *rac*-/LiHMDS[b] | 6.5 | 1.8 | 23.2 | 3.4 | 65.1 |
| *rac*-/**6**(50:1) | 9.3 | 6.5 | 12.2 | 7.0 | 65.1 |
| *rac*-/**6**(75:1) | 10.1 | 6.6 | 12.9 | 6.4 | 64.1 |
| *rac*-/**6**(50:1)[b] | 6.7 | 1.9 | 20.8 | 3.9 | 66.7 |
| *rac*-/**6**(100:1) | 10.0 | 6.7 | 13.0 | 6.3 | 63.9 |
| *rac*-/**6**(150:1) | 10.0 | 6.4 | 13.0 | 6.3 | 64.2 |

[a] ht = heterotactic; sb it = stereoblock isotactic; it = isotactic. [b]Dichloromethane as solvent.

**Table S2**. Theoretical NMR and experimental MW values for cPLAs.

| Entry | LA, Catalyst | $[LA]_0/[Cat]$ | Exp.$M_w$ (kDa)[a] | Theoretical Mn (kDa)[b] |
|---|---|---|---|---|
| 1 | L-, LiHMDS | 50:1 | 29.0 | 15.0 |
| 2 | L-, LiHMDS[c] | 50:1 | 25.4 | 28.8 |
| 3 | L-, **6** | 50:1 | 49.5 | 10.3 |
| 4 | L-, **6**[c] | 50:1 | 79.3 | 35.7 |
| 5 | L-, **6**[d] | 50:1 | 51.4 | 20.3 |
| 6 | L-, **6** | 75:1 | 72.1 | 34.4 |
| 7 | L-, **6** | 100:1 | 94.6 | 37.6 |
| 8 | L-, **6** | 150:1 | 137.6 | 52.8 |
| 9 | L-, **6** | 300:1 | 179.6 | 58.5 |
| 10 | *rac*-, LiHMDS | 50:1 | 15.2 | 12.7 |
| 11 | *rac*-, **6** | 50:1 | 24.7 | 18.8 |
| 12 | *rac*-, **6** | 75:1 | 48.7 | 28.9 |
| 13 | *rac*-, **6** | 100:1 | 55.9 | 33.1 |
| 14 | *rac*-, **6** | 150:1 | 90.0 | 45.2 |
| 15 | *rac*-, **6** | 300:1 | 85.6 | 11.1 |

[a] Determined by $^1H$ PGSE diffusion NMR using polystyrene standards and without the use of any correction factor. [b] Obtained by dividing the integral of the 5.1 ppm signal (assigned to the internal lactide unit) by the integral of the 4.3 ppm signal assigned to the terminal lactide unit. [c] Dichloromethane as solvent. [d] In-situ formation by stirring LiHMDS and ligand **5** for 1 minute at room temperature prior the addition of LA.

**Table S3**. Diffusion coefficients and weight-average molecular weights (Mw) estimated via dART, TRAIn and LMS procedures. PDI values are also provided. Both maxima and average values of the solutions are given for dART and TRAIn methodologies.

| | LiHMDS | | LiAQ (**6**) | |
|---|---|---|---|---|
| | L-cPLA | *rac*-cPLA | L-cPLA | *rac*-cPLA |
| $D^{dART}$ ($10^{-9}$ $m^2$ $s^{-1}$) max | 0.1118 | 0.1437 | 0.0772 | 0.1491 |
| $D^{TRAIn}$ ($10^{-9}$ $m^2$ $s^{-1}$) max | 0.1087 | 0.1439 | 0.0770 | 0.1469 |
| $D^{dART}$ ($10^{-9}$ $m^2$ $s^{-1}$) average | 0.0940 | 0.1358 | 0.0688 | 0.1026 |
| $D^{TRAIn}$ ($10^{-9}$ $m^2$ $s^{-1}$) average | 0.0961 | 0.1323 | 0.0668 | 0.1087 |
| $D^{LMS}$ ($10^{-9}$ $m^2$ $s^{-1}$) | 0.0917 | 0.1304 | 0.0666 | 0.0990 |
| $MWw^{dART}$ (Da) max | 18711 | 12019 | 35853 | 11465 |
| $MWw^{TRAIn}$ (Da) max | 19646 | 12859 | 36081 | 11561 |
| $MWw^{dART}$ (Da) average | 25921 | 14056 | 44722 | 22134 |
| $MWw^{TRAIn}$ (Da) average | 24403 | 13781 | 46284 | 19995 |
| $PDI^{TRAIn}$ | 1.24 | 1.27 | 1.27 | 1.23 |
| $MWw^{LMS}$ (Da) average | 26972 | 14514 | 47355 | 23570 |

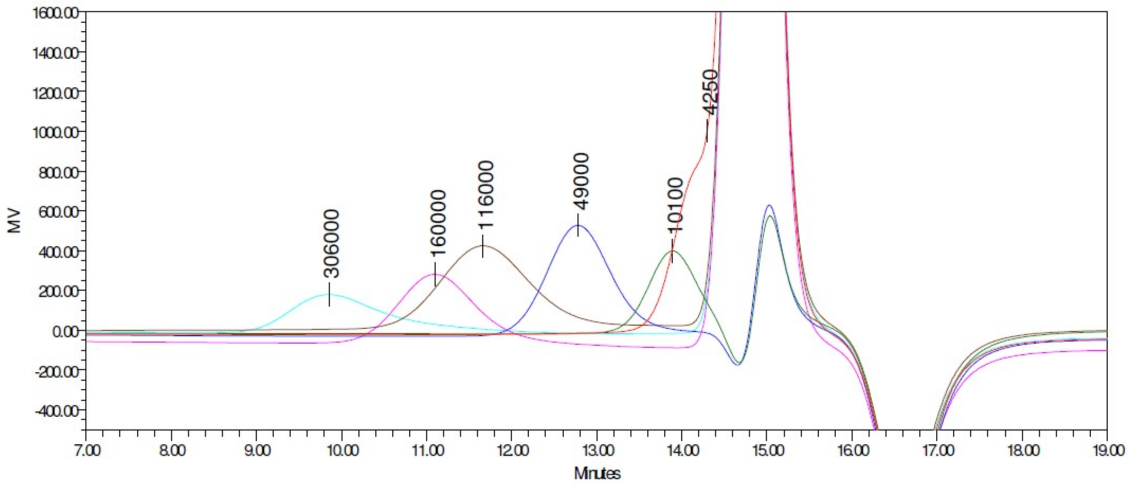


| | SampleName | Injection | RT | MP (Daltons) |
|---|---|---|---|---|
| 1 | STD PMMA 300.000 | 1 | 9.852 | 306000 |
| 2 | STD PMMA 150.000 | 1 | 11.099 | 160000 |
| 3 | STD PMMA 100.000 | 1 | 11.665 | 116000 |
| 4 | STD PMMA 50.000 | 1 | 12.780 | 49000 |
| 5 | STD PMMA 10.000 | 1 | 13.894 | 10100 |
| 6 | STD PMMA 4.000 | 1 | 14.300 | 4250 |

**Figure S17**. Overlap of all the PMMA chromatograms employed in SEC analysis.

## GPC Calibration Curve Information

| | | | | | |
|---|---|---|---|---|---|
| Date Calibrated: | 1/27/2021 10:37:04 AM CET | A: | 3.636074e+001 | D: | -2.236132e-002 |
| Processing Method: | PLA 3ordre cal | B: | -8.155815e+000 | E: | 0.000000e+000 |
| Fit Order: | 3 | C: | 7.300512e-001 | F: | 0.000000e+000 |
| Cal Curve ID: | 1221 | R: | 0.999983 | R^2: | 0.999967 |
| | | v0: | 6.000000 | vt: | 16.000000 |

Adquirit per Eva María del Álamo Dr. Isidre Casals

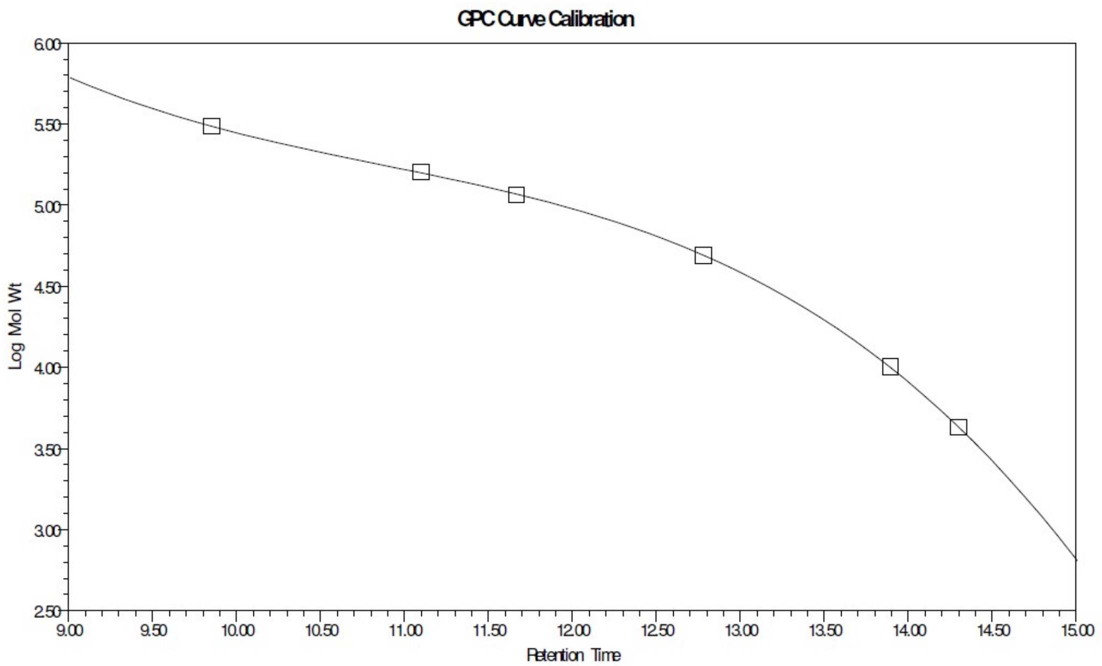


## GPC Calibration Table

| | Retention Time (min) | Mol Wt (Daltons) | Log Mol Wt | Calculated Weight (Daltons) | % Residual |
|---|---|---|---|---|---|
| 1 | 9.852 | 306000 | 5.4857 | 306617 | -0.201 |
| 2 | 11.099 | 160000 | 5.2041 | 158143 | 1.174 |
| 3 | 11.665 | 116000 | 5.0645 | 117240 | -1.057 |
| 4 | 12.780 | 49000 | 4.6902 | 49169 | -0.343 |
| 5 | 13.894 | 10100 | 4.0043 | 9981 | 1.194 |
| 6 | 14.300 | 4250 | 3.6284 | 4282 | -0.743 |

**Figure S18**. SEC Calibration curve based on six PMMA standards.

a) b) c) d)

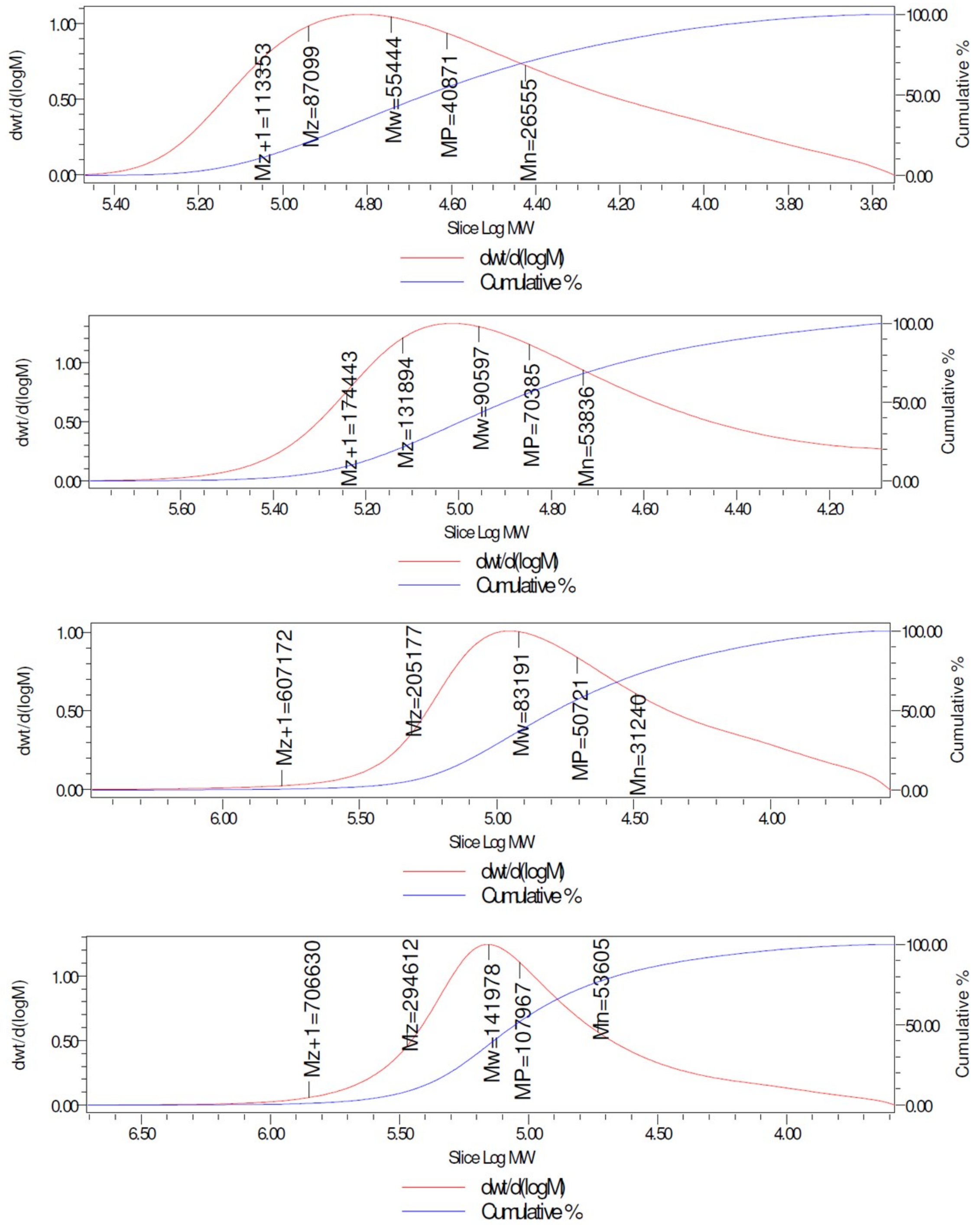


**Figure S19**. SEC mass distribution curves for entries 1-4, Table 3 (see manuscript).

e)

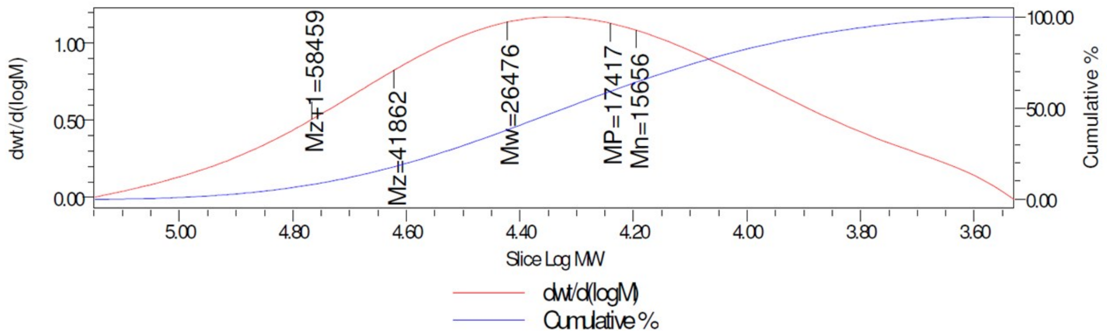


f)

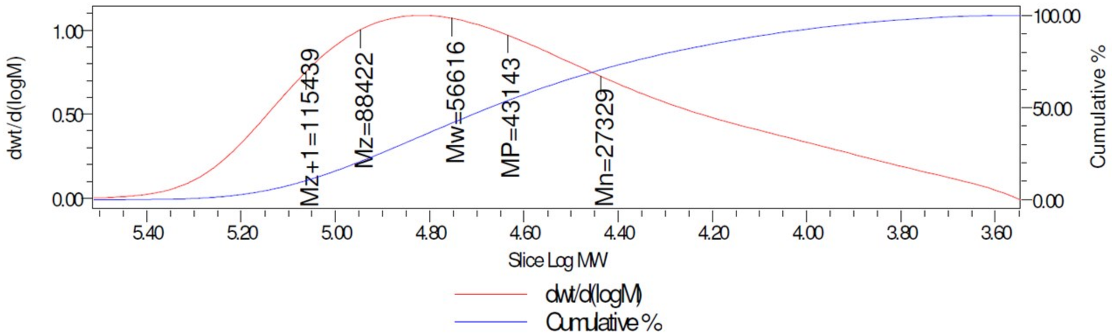


g
)

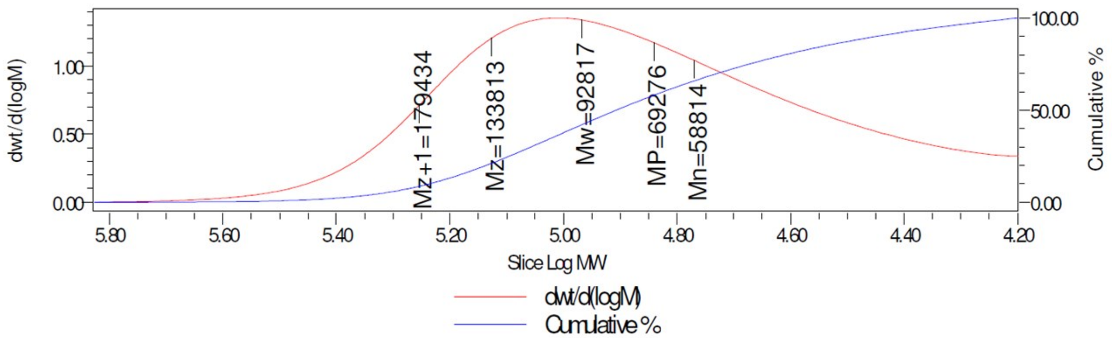


**Figure S20**. SEC mass distribution curves for entries 5-7, Table 3 (see manuscript).

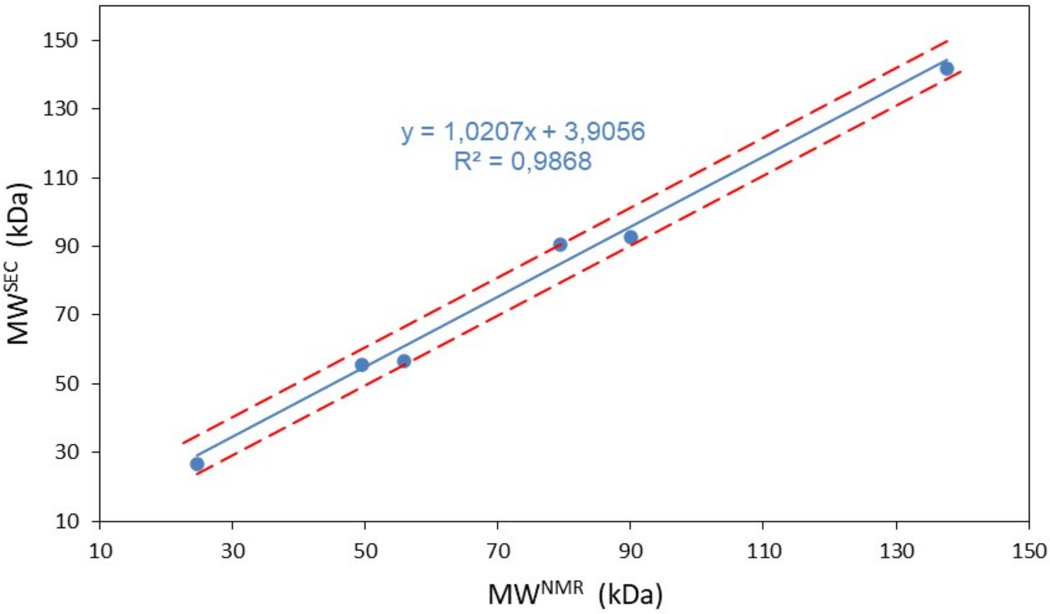


**Figure S21**. Comparison between Mw retrieved from NMR diffusion measurements on cPLA samples in CDCl3 dilute solutions (c ≈ 1.7 wt%) and those obtained by SEC. The two dashed lines indicate the range with a Mw confidence of 95%. The intercept obtained is 3.9056, with the upper and lower confidence limits of 12.4165 and -4.6053. The slope of the graph is 1.0207, with the 95% confidence interval of 1.1272–0.9142.